

Modelling and simulating a high-resolution high-fidelity model for three discoveries in the Måløy Slope, Norwegian North Sea

Adnan Khalid^{1*}, Pablo Cifuentes¹, Pedro Duran¹, Philippa Park¹, Arthur Satterley¹, Stefan Calvert¹ and Carolina Coll¹ present a high-resolution high-fidelity model of the Måløy Slope area integrating the operators' geological interpretations along with CGG's petrophysical analysis and high-resolution seismic inversion results.

Introduction

The importance of detailed reservoir characterization and modelling for accurate reservoir performance prediction has always been recognized, but generally it is necessary to upscale reservoir properties derived from seismic data to create models that can be run in a reasonable timeframe and are a useful tool for prediction. CGG has combined its strengths in high-resolution seismic imaging and its high-performance computing (HPC) capability into a new modelling workflow which allows preservation of the high-resolution seismic information directly within the dynamic reservoir simulation model. These models can be used for field development planning and production optimization. There is no requirement to upscale the seismic-derived parameters and the models can be run effectively in a reasonable time frame.

The benefits of this approach are considerable as volumetric displacement efficiency can be strongly affected by small/medium-scale heterogeneity and connectivity. However, dynamic reservoir models are usually built at log resolution in the vertical direction, but at a coarser resolution laterally and often upscaled vertically. This is due to the impact that maintaining seismic resolution laterally can have on the reservoir model size and, as a consequence, run times. The full potential of the high-resolution seismic, acquired at a high cost for the operator, is not used to its maximum value to model reservoir heterogeneity and connectivity at a fine scale. With the use of a high-fidelity model (HFM), tasks which previously benefited from the use of a sector model for fine scale, such as enhanced oil recovery (EOR) simulation, can now be performed in the full field model where it is easier to apply appropriate constraints on production and boundary conditions. History-matching can be made more straightforward as there is no requirement for local grid refinements to match well test data. Flood fronts can be modelled with more vertical and areal resolution, achieving better sweep estimation, and improving the understanding of hydrocarbon volume distributions for well drilling optimization and identification of bypassed oil.

Using CGG's North Viking Graben (NVG) PSDM multi-client high-resolution seismic dataset, CGG's team created a

high-resolution HFM of the Måløy Slope area integrating the operators' geological interpretations of the area along with CGG's petrophysical analysis and high-resolution seismic inversion results. Engineering information observed during drilling and testing of the discoveries in this area was history-matched. Several static model scenarios were generated to evaluate resources uncertainty. A HFM was built for a mid-case scenario (base case) and history-matched. Using the history-matched model, potential development scenarios were investigated. This demonstrates how the base-case HFM was used to best optimize future drilling locations, as well as optimize the field development plan to achieve optimum technical recovery of hydrocarbons and assess the impact of key uncertainties for future development planning. The following sections summarise the workflows and results of this study, as well as the results of the runs, using CGG's high-performance computers.

Background

The first discovery well 35/3-2 in the Måløy Slope (Northern North Sea) was drilled in 1980 by BP, who were a licence partner at that time. The well successfully tested gas condensate in the Agat Formation (Cretaceous). During the Drill Stem Test (DST) the well flowed at 1,082,000 sm³/d (38.2 MMSCFD) through a 38/64" choke and a final flow rate of 736,000 sm³/d (26 MMSCFD) through a 32/64" choke. Repeat Formation Tester (RFT) measurements indicate a Gas Water Contact (GWC) at 3584.5 mBRT (3558.5 mTVDSS). The gas also produced condensate at a Condensate to Gas Ratio (CGR) of 10 BBLS/MMSCF along with 24 BWPD of condensed water. Produced condensate had API of 42° and gas gravity was recorded as 0.62.

Saga Petroleum followed this discovery by drilling well 35/3-4 in 1980-1981. This well also successfully tested gas condensate in the Agat Formation. The well delivered a stable gas flow rate during the first main flow period of 688,000 sm³/d (24.3 MMscfd) and the condensate flow rate was 84 sm³/d (528 BCPD) on a 36/64" choke. Produced CGR was ca. 26 BBLS/MMSCF and produced gas gravity was 0.62. Condensate gravity was 45.4°

¹ CGG

* Corresponding author, E-mail: adnan.khalid@cgg.com

DOI: 10.3997/1365-2397.fb2022078

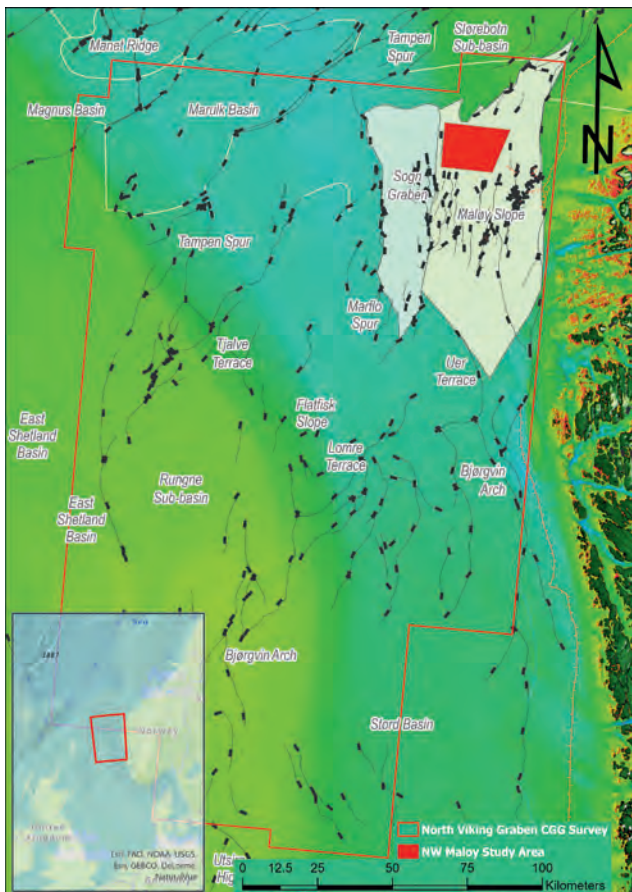


Figure 1 Northern Viking Graben location map. The red polygon outlines the study area over the NW of the Måløy Slope.

API. PVT samples were taken from this well and PVT lab reports are available for the produced fluid. RFT measurements indicate a pressure-isolated gas-bearing upper zone and a water-bearing lower zone. A GDT was assumed at 3450 mTVDSS.

Then, VNG Norge AS drilled well 35/3-7S in 2009. MDT measurement indicates a GWC at 3553 mTVDSS. Estimated gas and water gradients were 0.153 psi/ft and 0.444 psi/ft respectively. No DST or PVT sampling was performed.

Between 2014 and 2018 CGG acquired a north-south 44,000 km² 3D broadband high-resolution survey over the North Viking Graben (NVG) area of the Northern North Sea. The Måløy Slope is located in the northeast of the NVG survey. CGG’s broadband acquisition and imaging solution (Soubaras et al., 2012) was used to deliver detailed high-resolution subsurface images with the best low frequencies through a combination of advanced equipment, and proprietary pre-stack source and receiver deghosting and imaging technology. CGG’s technology enables the recording of a full range of frequencies, low as well as high, which is key to increasing the resolution of both the shallow and deeper parts of the seismic section.

Static model building

A static model was built in a study area covering almost 300 km of the Måløy Slope. The Måløy Slope is bounded to the west by large west-dipping normal faults that form the eastern margin of the Sogn Graben (Figure 1), and to the east by the Øygarden Fault Complex (Prélat et al., 2015).

The targeted reservoir corresponds to the Albian Agat Formation, which consists of stacked turbiditic submarine fans. The Agat Formation was fed from the eastern hinterland areas (mainland Norway) and transported across the shelf westward. Sediment was fed through canyons over west-dipping normal faults and deflected by relay ramps. This scenario shaped an inter-channel setting, generating a high sedimentological variability from sandy channel deposits to hemipelagic muds associated with small terminal fans downslope.

Several static deterministic models were generated using different weights on the influence of the seismic data during rock property modelling (Co-kriging) in order to assess its impact on connectivity and volumetric uncertainty. More sophisticated uncertainty methods can be used to assess reservoir uncertainty (e.g., global optimization, ensemble methods) which will produce hundreds of realizations from which mid (P50), low (P90) and high (P10) scenarios can be selected to build deterministic HFM models that can be used for development planning optimization and reserves/resources estimations (Coll, C., 2019).

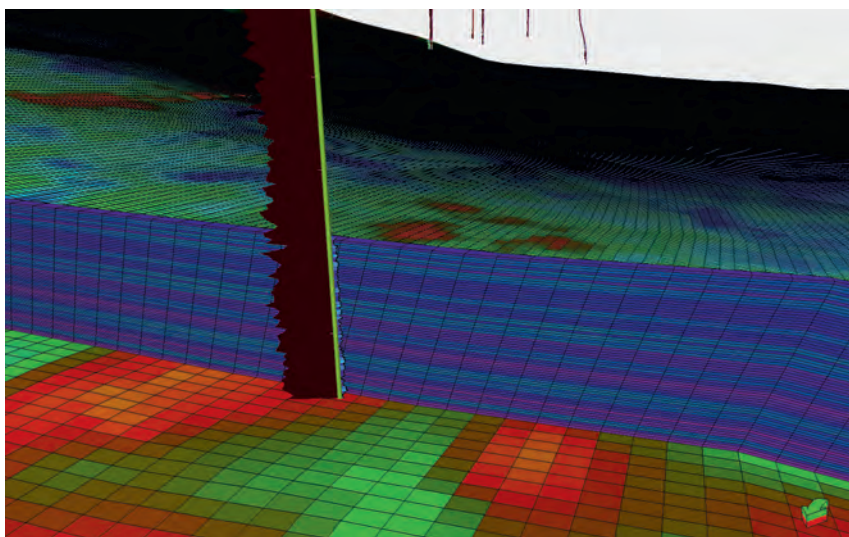


Figure 2 High-resolution grid that combines the high-resolution information from the seismic volume (acoustic impedance displayed in the K direction) with a vertical resolution determined by well log data (Porosity display in the J direction).

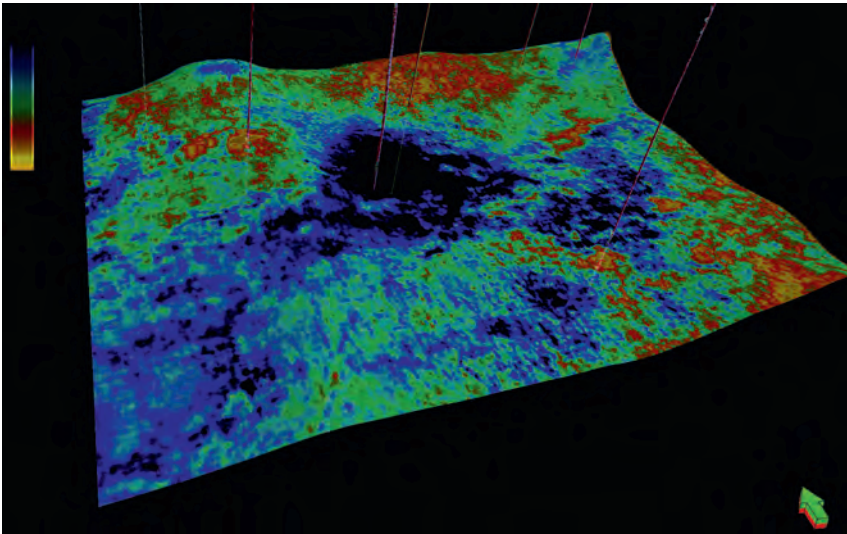


Figure 3 High-resolution grid displaying acoustic impedance along the area of the study.

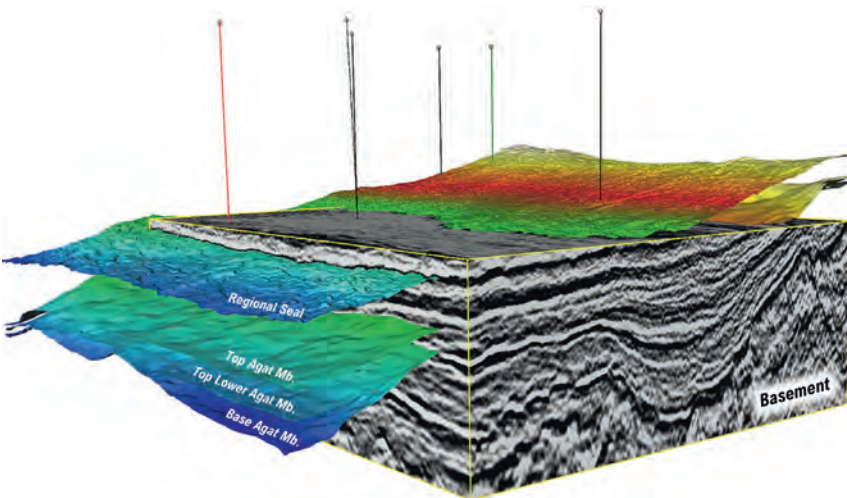


Figure 4 Image showing the seismic dataset used for the high-fidelity model reservoir, wells and the top seal, top, intra-Agat member and base reservoir.

The static model was built honouring the horizontal seismic resolution (12.5x18.75m) and the well vertical sampling (1.25 m) of the broadband NVG survey (Figure 2). This high-resolution seismic makes it possible to capture the key geological features at a medium scale with the interpretation showing reservoir heterogeneity and connectivity. By following this methodology, seismic data and resolution was fully incorporated into the static model, honouring the high resolution offered by the quality of the seismic dataset (Figure 3).

The first step in the static modelling was to perform structural interpretation, Figure 4. The workflow included an evaluation of the lateral evolution in the relay ramps and other types of fault linkage followed by the top and base Agat Formation. Based on the geometries revealed by these two horizons, a third horizon named Intra-Agat was picked to distinguish between the first stages of Agat sedimentation (where deposition is influenced by the inherited paleogeography created by large west-dipping normal faults) and a later stage in which antecedent topography was blanketed. Finally, the interpretation of the regional seal, the Svarte Formation, was carried out to gain a full picture of the reservoir architecture. These Cenomanian sediments consist of calcareous mudstones interbedded with chalky limestones. The proportion of limestone gradually decreases northwards towards the Måløy Slope (Surlyk et al., 2003).

Petrophysics

Four wells were re-interpreted from the NPD database (35/3-2, 35/3-4, 35/3-5 and 35/3-7S). A standard shaly sand approach was taken applying the Modified Simandoux S_w equation to all four wells. Generally, log quality was poor due to adverse wellbore conditions. This required some log cleaning and normalisation of the gamma log, mainly due to the vintage of the data. This approach allowed a common basis for comparison and input into the static model for the Agat sands. The vertical resolution of the upscaled logs was 1.25 m used as the vertical resolution for the geological and simulation grid (Figure 2).

Seismic inversion

A deterministic acoustic inversion targeting the Agat formation was performed in the time domain using the latest version of the seismic data and CGG's proprietary workflows. The initial model was built for an area of 1500 km² that covers different fields in the area based on prospectivity. The horizons used to build the initial model were interpreted as part of the present project and include the Top Svarte Formation, Top Agat, Intra-Agat and the Top Åsgard Formation. A total of seven wells were included in the initial seismic inversion model, four of which are located inside the target area for the high-fidelity model (Figure 3).

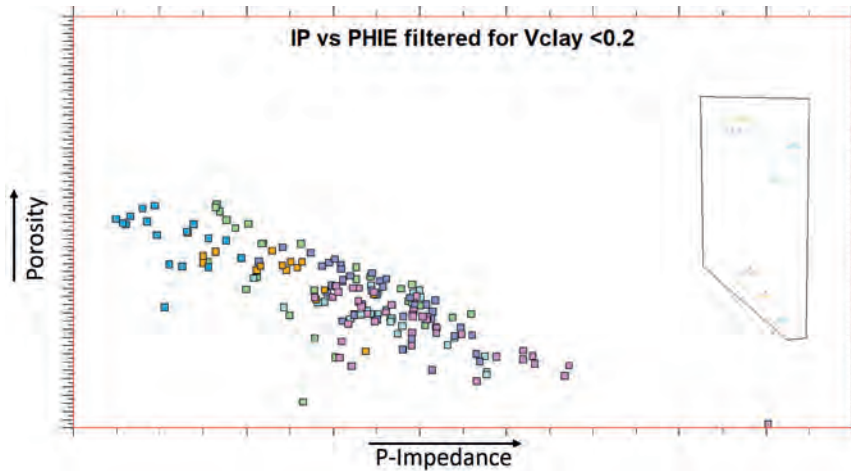


Figure 5 Cross-plot Impedance vs Porosity for clean sands in the inversion area.

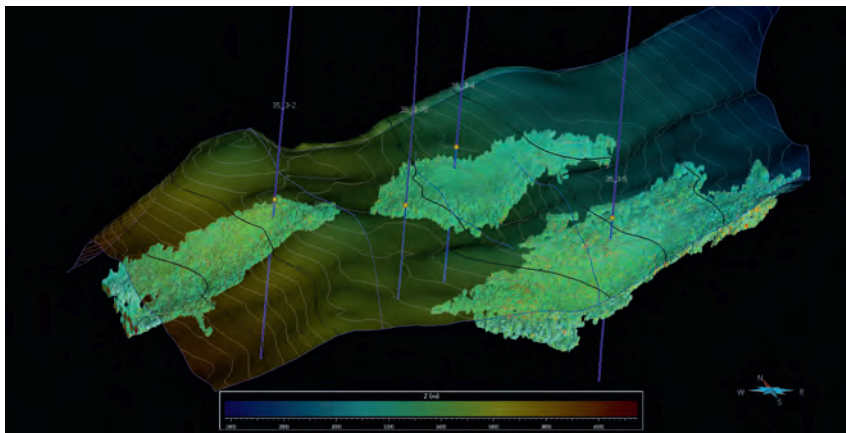


Figure 6 Geobodies based on low I_p values.

Inversion results were converted to depth using a calibrated velocity model that honoured the well markers in the depth domain. A cross plot of acoustic impedance (I_p) and porosity showed a correlation that was used during the modelling stage, in this case for the clean sand (Figure 5). In addition, lateral variations in the impedance values between the north and south areas are observed which suggests a lateral variation in the properties over the inversion area.

Geobodies for the entire area were extracted based on criteria developed during the inversion as seen in the image (Figure 6). The geobodies enable identification of different prospective areas with potential to have good porosity, and some of these geobodies are in the area of drilled wells 35/3-2, 35/3-4, 35/3-7S. Independent of this study, a new appraisal well drilled by Neptune Energy Norge AS in the area (ref: Norwegian Petroleum Directorate, 2022) intersected one of the prospective geobodies identified by our inversion results.

Reservoir engineering

The regional RFT/MDT interpretation for wells 35/3-2, 35/3-4, 35/3-7S and 35/3-5S highlights the complexity of these areas and the need for a maximum leverage of the high-resolution seismic data. For well 35/3-4, RFT measurements in the Lower Cretaceous indicated an upper zone with a gas gradient of 0.123 psi/ft and a deeper zone with a water gradient of 0.45 psi/ft. There is no pressure communication between these two zones. Well 35/3-7S seems to have no pressure communication with

well 35/3-4. The dry well 35/3-5S has a similar pressure profile as 35/3-7S. While the pressure profile for wells 35/3-4, 35/3-7S and 35/3-5S was slightly different, the pressure for 35/3-2 was ca. 1350 psi higher than 35/3-7S which stands out as an anomaly. These results suggest a compartmentalized area with isolated fault blocks or sand bodies with different pressure regimes. Figure 7 shows the regional MDT plot.

A Pressure Transient Analysis (PTA) interpretation was performed for well 35/3-4 to evaluate the ability of the HFM to be history-matched with less modifications to the reservoir properties by better representing the lateral heterogeneity. Of all the models used, the bounded model with three sealing faults gave a good match while being geologically plausible according to the high-resolution geological model. The flow capacity (Kh) estimated by this analysis was ca. 1260 md-ft. The operator's assessment for well 35/3-2 was reviewed and the analysis indicated the presence of two sealing faults in the vicinity of the well and a Kh of 1130 md-ft.

Geo-modelling

A high-resolution grid was built for the sector area around wells 35/3-2, 35/3-4, 35/3-7S. The internal reservoir architecture is controlled by an intermediate horizon (Intra-Agat) and the areal distribution of the properties is controlled by the high-resolution seismic inversion results.

High seismic resolution (12.5m by 18.75m) is preserved in the horizontal resolution of the grid and the vertical resolution

(1.25 m) is defined in a traditional way from a well facies log (see Figure 2). This provides a high level of detail that combines the vertical resolution from the well logs with the lateral resolution from the seismic data. The selected area (Figure 6) has around 160 million grid blocks, helping to better define reservoir heterogeneity and reducing uncertainty in the reservoir properties along the area and enabling a better understanding and interpretation of the reservoir and the fluid flow behaviour in it.

Static properties, such as porosity and vshale, were modelled using well information as hard data and the inversion results as secondary data. Rock quality was derived from porosity and vshale cutoffs, and the permeability-porosity relationship was derived from core data cross-plot analysis using different correlations per facies (clean sand, shaly sand and shale) and per formation (Upper Agat and Lower Agat) that helped to understand flow units. Seismic inversion results highlighted variability in rock properties along the entire inversion area, making it possible to define some prospective geobodies which were used to delineate the location of the simulation model (Figure 2).

Dynamic model and stability test

Since wells 35/3-2, 35/3-4 and 35/3-7S are in different pressure regimes, the dynamic simulation model was divided into three different regions (Segments 35/3-2, 35/3-7S and 35/3-4) separated by two major North-South faults providing the pressure isolation between the regions. This is an area with complex fluid distribution that could not be explained with the existing models (Figure 7). The dynamic model was built in the selected NW area. The Lower Agat (as it is all in water) as well as the shale separating the Upper Agat and Lower Agat was discarded. Other reductions were due to shales in the Upper Agat and non-connected net reservoir in the shallow layers below the cutoff for minimum Hydrocarbon Pore Volume (HPV). The total number of active cells left in the simulation model was ca. 14.7 million. The model was initialized using equilibration.

For any simulation model, initialization and a stability test are important steps to ensure consistency of the input data and avoid unnecessary additional timestep calculations due to fluid movement and pressure changes between different cells

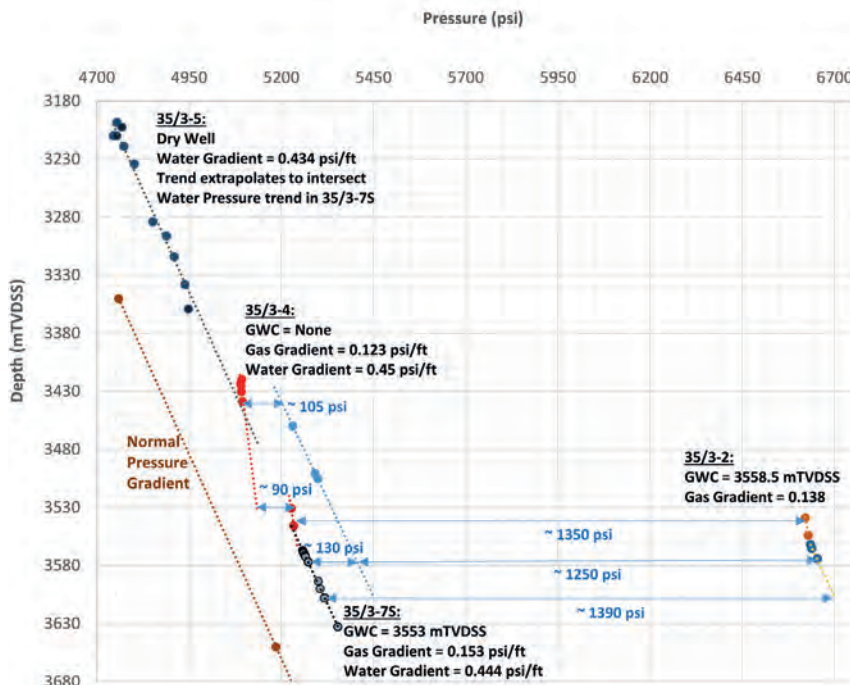


Figure 7 Regional RFT/MDT plot indicating different pressure regimes in the area of interest.

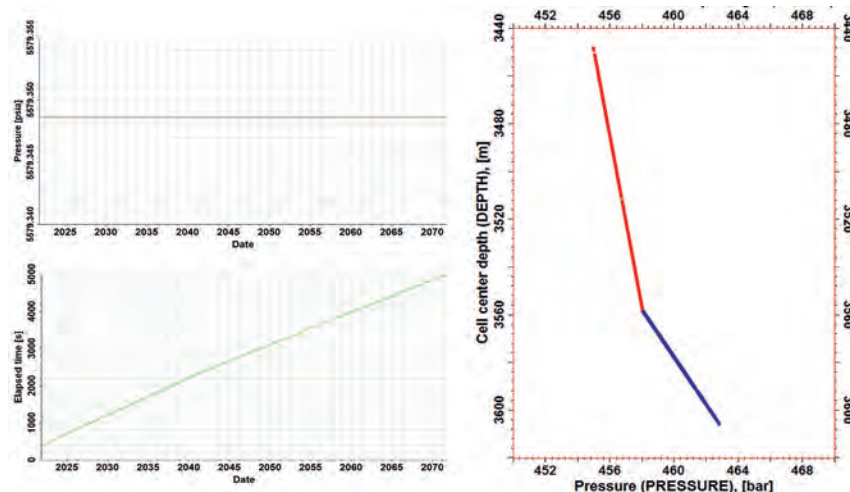


Figure 8 Top left: change in model pressure over a 50-year no production no injection stability test. Right: Pressure gradient in the model after 50-year stability test. Bottom left: Time taken to simulate 50-year stability test.

while attempting to achieve equilibrium. To test the stability of the model, a no production/injection test was performed with yearly timesteps for 50 years. The results of this test are shown in Figure 8 showing negligible pressure change over 50 years. The test was completed within reasonable simulation time per year using consistent time steps throughout indicating proper equilibration of reservoir fluids. The initial water saturation was compared to the water saturation at the end of the 50-year period and showed no changes in saturation over time.

History match

The HFM incorporates the heterogeneity observed from seismic inversion (Figure 9). RFT/MDT pressures had been reasonably

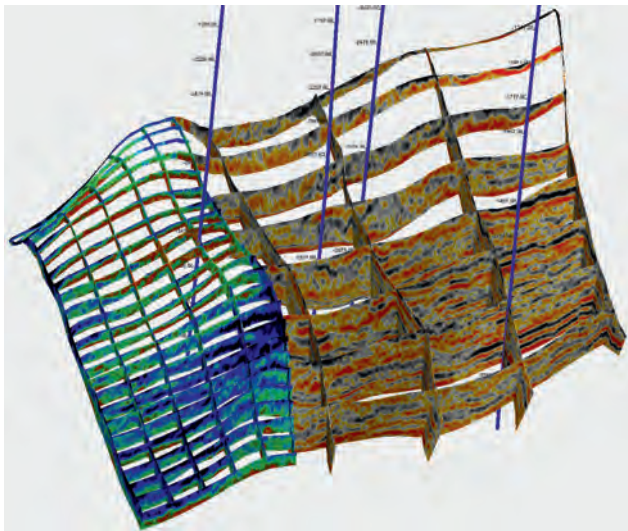


Figure 9 High-resolution grid with seismic information and inversion results showing reservoir heterogeneity.

matched at the onset of history matching after adjustments to the gas density for compartments which did not have a detailed PVT description based on near-field data. The porosity-permeability data from these wells was not originally corrected for overburden pressure. The initial history match cases indicated that the poro-perm relationship resulted in a higher Kh in comparison to observed Kh from the well tests. To get closer to observed Kh from pressure transient analysis (PTA), the poro-perm relationship was adjusted to correct for the overburden pressure until the Kh in the model and observed Kh were matched and comparable. Near wellbore effects such as faults and rate-dependent skin observed through PTA were also included in the simulation model which improved the pressure matches significantly. Figure 10 shows the matches achieved for well 35/3-4's RFT, rates, pressure and pressure derivative.

Field development plan and forecast predictions

Using the history-matched model, we investigated how the field development plan can be designed to optimize well locations, drainage area and reduce risks of potential interference between wells. Possible new locations for development wells were selected using hydrocarbon pore volume estimations (HuPhiSo), Bright Spot maps and recoverable volumes from the simulation model (Figure 11). HuPhiSo maps are generated by multiplying height, porosity and saturation of hydrocarbon for each cell in a layer and then these dimensionless cell values are summed up vertically to generate 2D maps. HuPhiSo maps were created for all three model regions. Using this map, a few locations were selected as possible locations for new wells. The high-resolution facies and property maps enabled identification of prospective areas for drilling new wells. Since

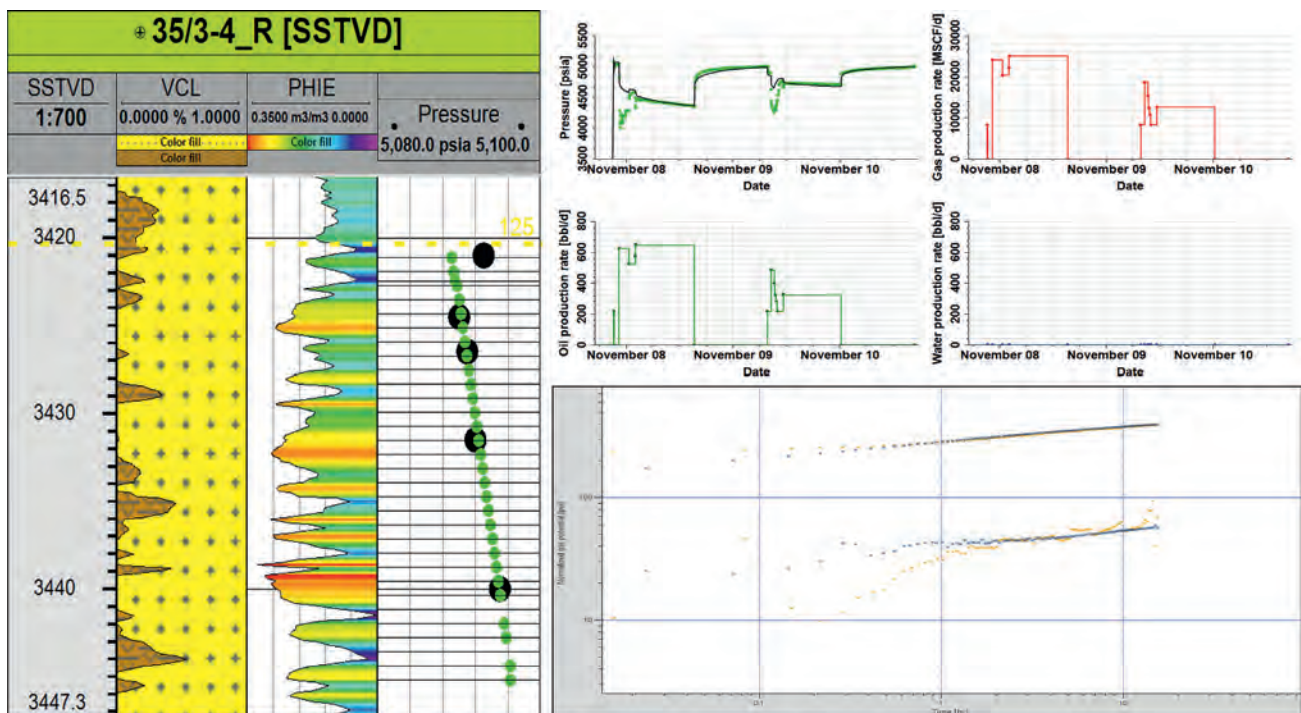


Figure 10 Left: RFT match for well 35/3-4 (Green dots simulated RFT, Black dots observed data points). Top Right: Drill Stem Test (DST) Rates and bottom hole pressure matches (Dotted points: Observed data; Solid lines: Simulated data). Bottom Right: Pressure and derivative for main build-up period match (Orange plus points: observed data pressure and derivative, Blue plus points: Simulator pressure and derivative).

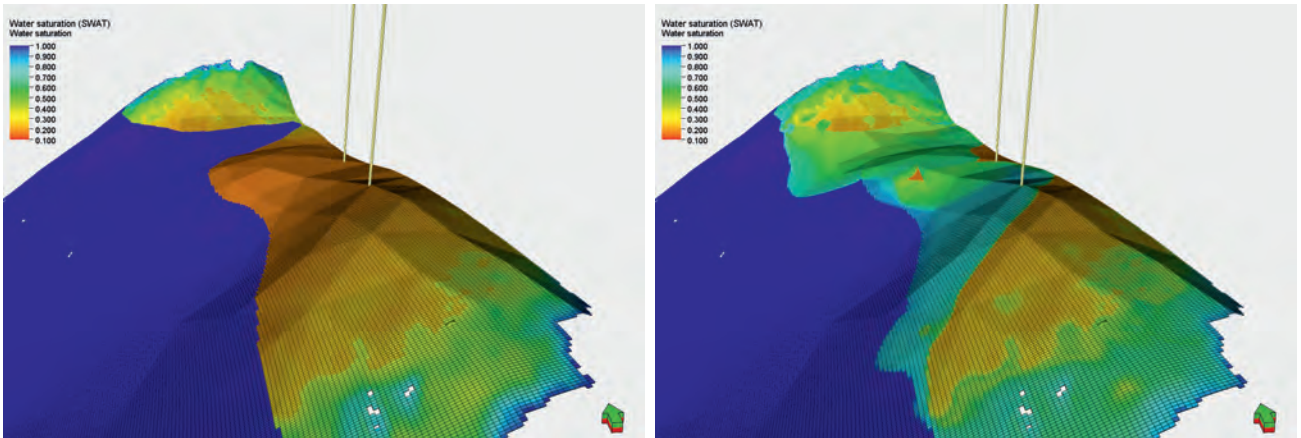


Figure 11 Water saturation at the start and end of the forecast prediction period in layer 73 using the final new well locations in Segment 35/3-2.

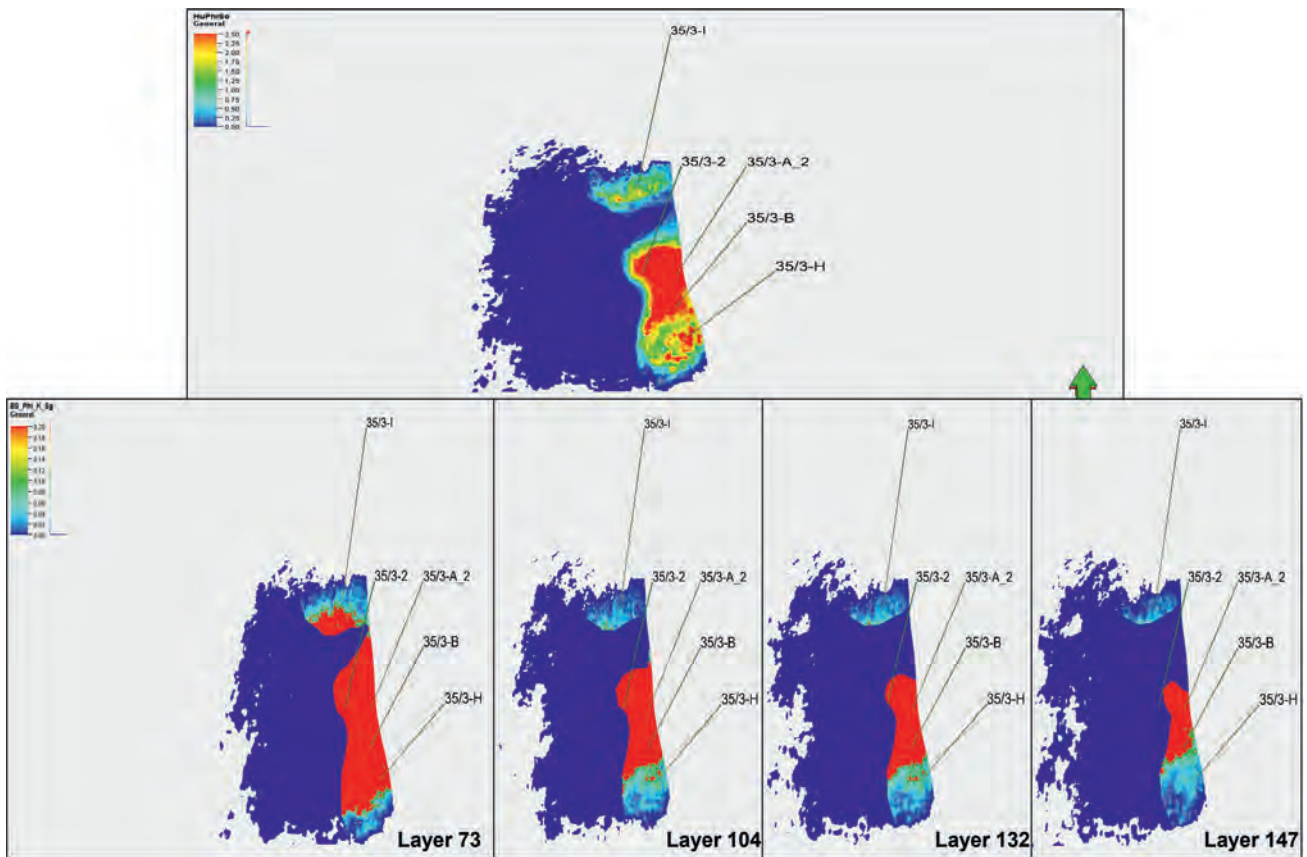
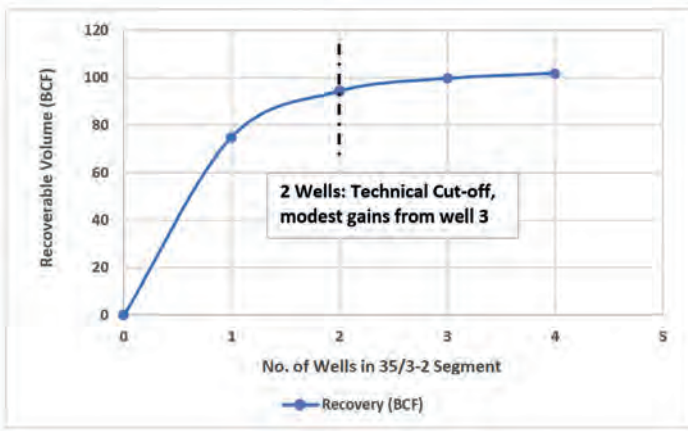


Figure 12 Top Image: HuPhiSo map for Segment 35/3-2 with discovery well and new well test locations. Red areas indicate areas of best porosity, gas saturation and thickness. Bottom image: Bright Spot maps with red areas indicating good porosity, permeability and saturation of gas for layers 73, 104, 132 and 147.

HuPhiSo maps do not consider the permeability of the selected location, Bright Spot maps which are multiples of porosity, S_g and permeability were used to fine-tune the well location. Figure 12 shows the HuPhiSo and Bright Spot maps for one of the segments in the model. New well locations were further fine-tuned for maximizing gas recovery by moving the wells closer to the faults and optimising well spacing based on the high-resolution property maps. The well count for each segment was optimized using a creaming curve as shown in Figure 13 for Segment 35/3-2. As observed in the creaming curve, wells I and H recoverable resources are small compared to wells A2 and B.

The same methodology was used to optimize the well count for segments 35/3-7S and 35/3-4 using vertical wells only. While segments 35/3-2 and 35/3-4 had comparable ca. 74% recoverable volumes from two and three vertical wells respectively, Segment 35/3-7S had a recoverable volume of 37% from two vertical well locations. Segment 35/3-7S is dominated by fine sand which has porosity in the range of 7-13%. The permeability in this region is low. For this reason, cumulative gas recovery from the vertical wells is lower in comparison to vertical wells in Segments 35/3-2 and 35/3-4 where the sand distribution is a mix of good-quality sand (higher than 13% porosity) and fine sand.



No. Of Wells	Well Locations	Recoverable Volume (BCF)
1	Well A2	75.0
2	Well A2 + B	94.3
3	Well A2 + B + I	99.6
4	Well A2 + B + I + H	101.8

Figure 13 Creaming curve for Segment 35/3-2 indicates that two wells (35/3-A2 and 35/3-B) are sufficient (technically) to recover 94.3 BCF gas which gives a recovery factor of 73.2%. Because of this analysis, well locations I and H were discarded since the recoverable volumes from those wells were not significant (as shown in the table above).

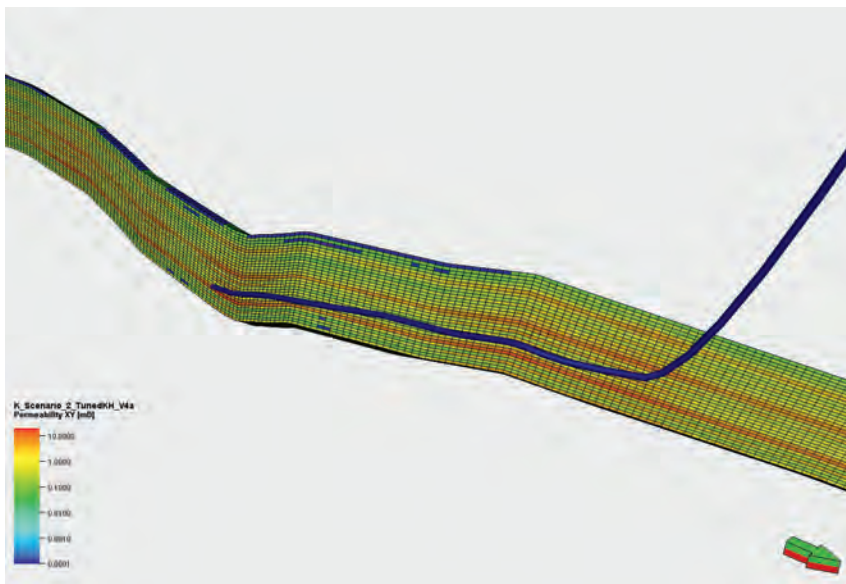


Figure 14 Image shows the new horizontal well placement for 35/3-D-H.

	Gas RF Without Aquifer	Gas RF with Aquifer
Segment 35/3-7S	60%	57.6%
Segment 35/3-2	73.2%	58.4%
Segment 35/3-4	74.1%	62.1%

Table 1 Gas recovery factors for each segment with and without aquifer support.

To improve recovery from this segment, horizontal wells of different tunnel lengths were tested in the same locations as vertical wells. A sensitivity analysis on the tunnel length for horizontal wells was also performed to see its impact on fluid recovery. The use of the HFM helped to optimize the well trajectory to maximize the recoverable resources associated with the well (Figure 14). Figure 15 shows that horizontal wells improve the gas recovery significantly from 37% to 60% in this segment using a horizontal tunnel length of 1500 ft. Based on the sensitivity analysis on tunnel length, it was decided to keep a 1500 ft tunnel length for well 35/3-C and a 2500 ft tunnel length for 35/3-D as the recoveries were the highest with these tunnel lengths.

Workovers to control the water production were also investigated by shutting off a section of water producing perforations at the appropriate time. It was observed as a result of this exercise that there was no meaningful increase in gas recovery by

performing these water shut-off workovers. The presence of an aquifer was identified as one of the key uncertainties. Therefore, to see the impact of an aquifer on the recovery of hydrocarbon fluids, an edge drive numerical aquifer was fitted to each segment. Average reservoir properties were used to define these aquifers and the volume of the aquifer was adjusted such that the water volume with aquifer was nine times more than without aquifer. Table 1 shows the impact of aquifer on the gas recovery factor.

With the HFM it was possible to define the best well locations, with a more accurate definition of the aquifer movement and a better prediction of recoverable well resources and remaining resources to optimise the field development plan.

Comparison of predictions from HFM and coarse grid model

To illustrate the effect of using a fine grid simulation model on reservoir performance prediction, the HFM was coarsened by a factor of 4 in the I and J direction and by a factor of 2 in the K direction. This would translate to grid dimensions of 48 m, 75 m and 2.5 m in the I, J and K directions respectively. As a result of this, the active cell count in the model reduced from 14.7 million to ca. 0.55 million cells taking into account all the inactive cells. The coarse model had comparable initial volume in-place to

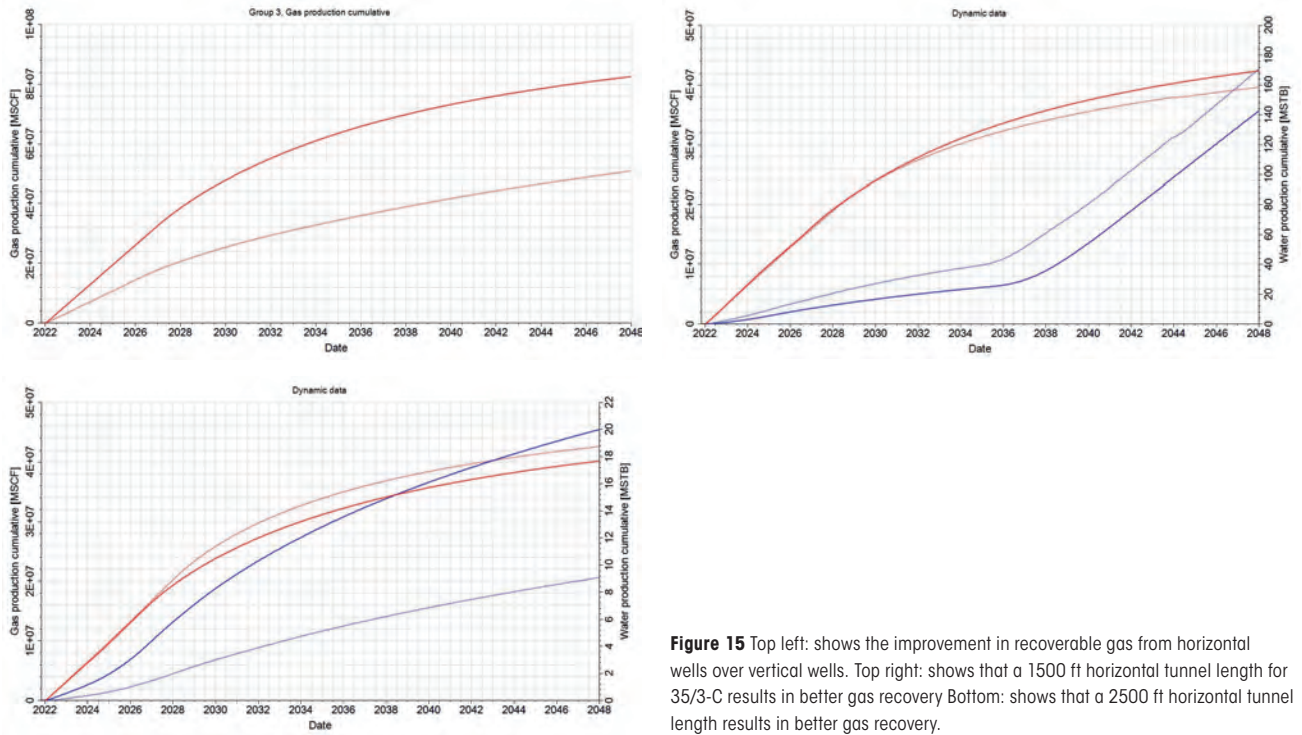


Figure 15 Top left: shows the improvement in recoverable gas from horizontal wells over vertical wells. Top right: shows that a 1500 ft horizontal tunnel length for 35/3-C results in better gas recovery Bottom: shows that a 2500 ft horizontal tunnel length results in better gas recovery.

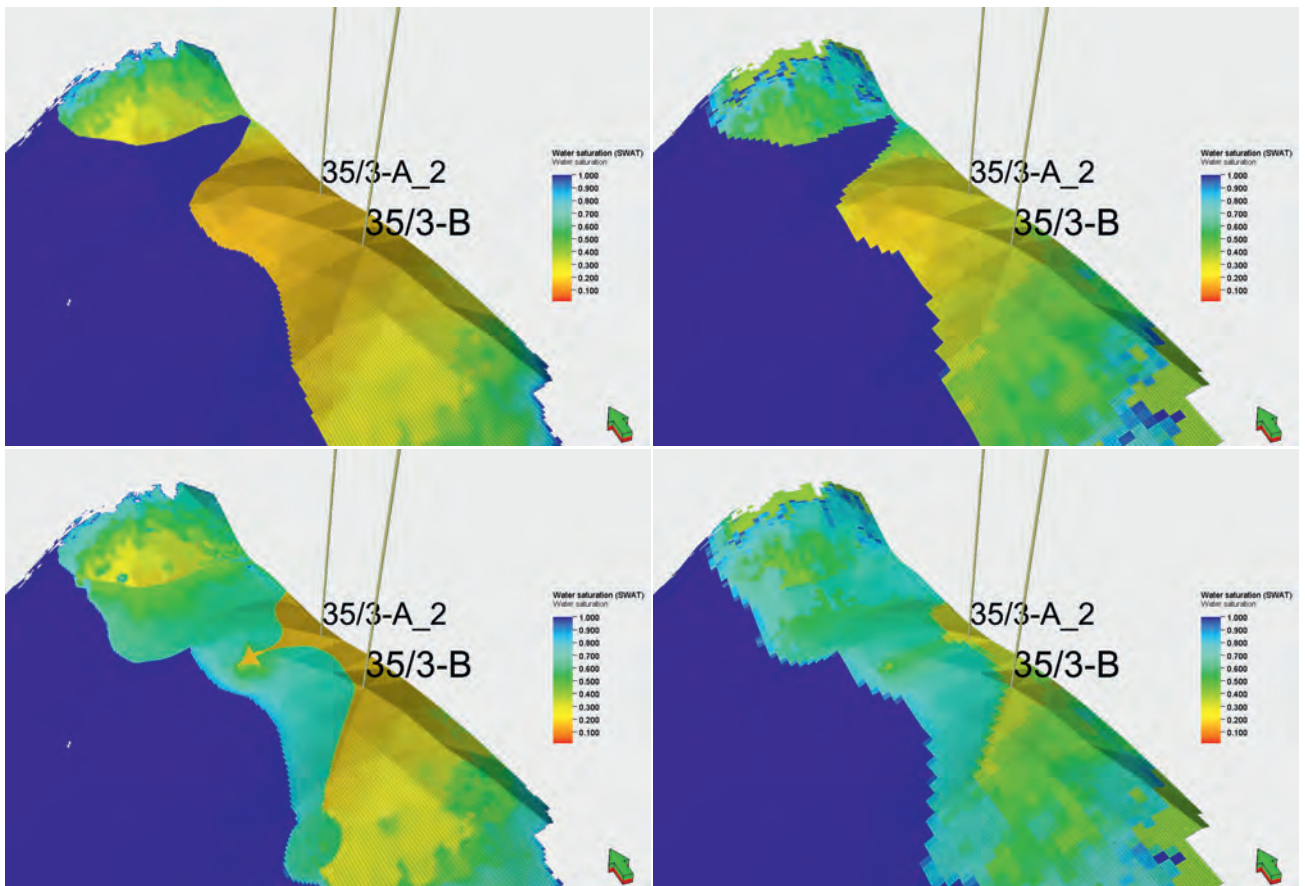


Figure 16 Comparison of water flood movement over time (2021 and 2036) in HFM (left) and coarse grid (right).

HFM. The coarse model was simulated with the same new well locations under similar forecast constraints as in HFM for a period of 25 years. Comparing the changes in saturation of water over time (Figure 16), it was observed that water flood movement

is faster in the coarse grid compared to the fine scale grid in HFM as expected due to the homogenization in the coarse grid reducing the areal and vertical heterogeneity. Figure 17 shows the movement of water flood along a cross-section in the I direction

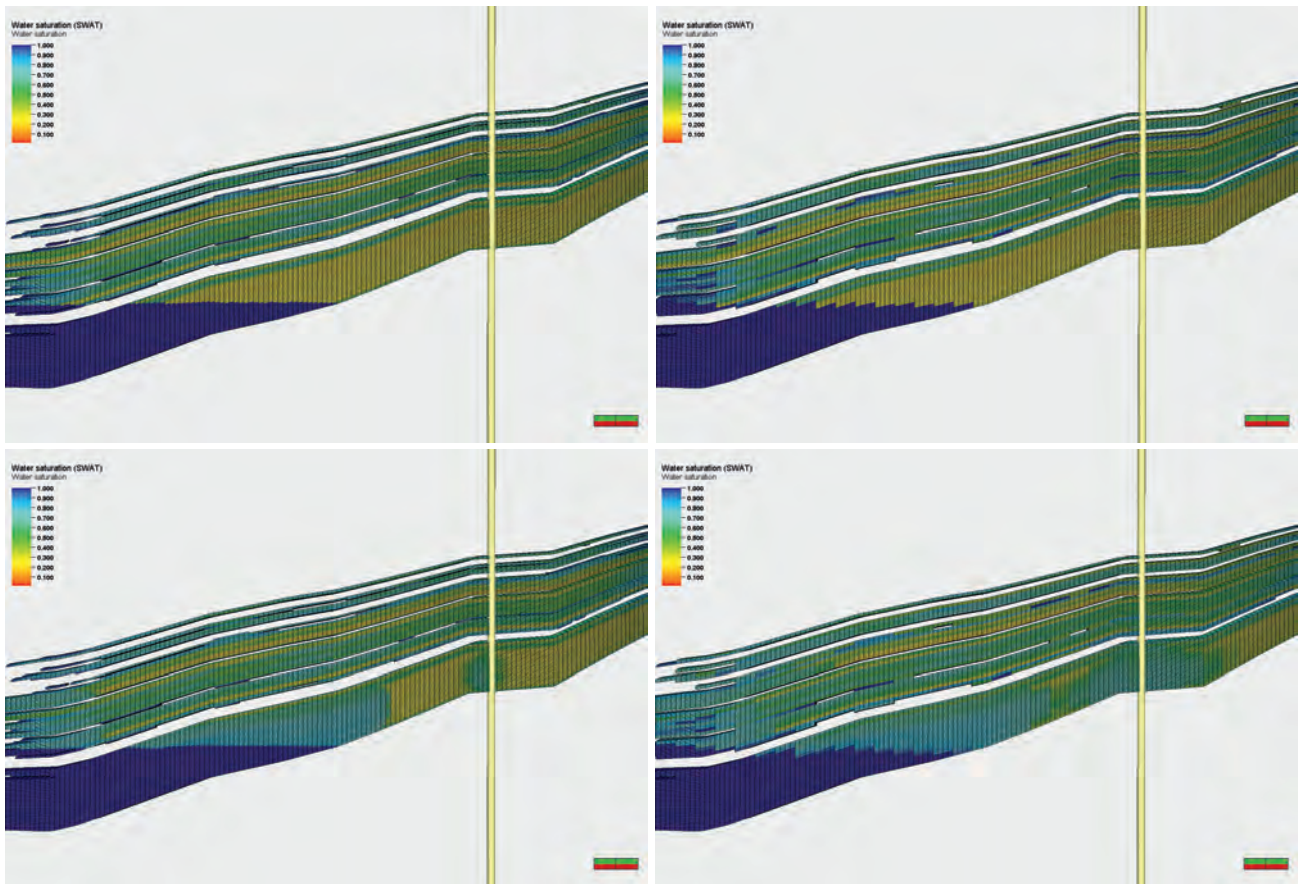


Figure 17 For well A2, comparison of water flood movement over time (2021 and 2036) in HFM (left) and coarse grid (right).

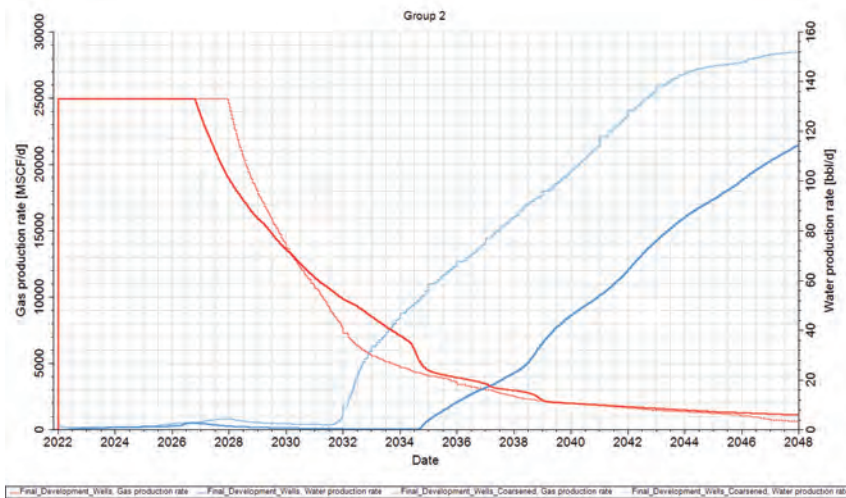


Figure 18 For Segment 35/3-2, comparison of gas and water production rates in HFM (solid red for gas and solid blue for water) and coarse grid simulation (dotted red for gas and dotted blue for water).

across well A2 for both a coarse and fine grid. It can be observed that as expected the water flood moves faster in the coarse grid compared to the fine grid. To reinforce this observation, for the two wells in this region, Figure 18 shows that the water breakthrough was approximately 2.5 years earlier in the coarse grid than the fine grid. This will have consequences for water handling facilities design during field development planning. In addition to this, the gas plateau rate duration is overpredicted by a year for the coarse grid which will have an economic impact during field development planning and production forecast. The fine grid model shows less acceleration of the recoverable volumes

due to the impact of more heterogeneity in the model. All these observations support the use of fine-scale HFM fully integrating high-resolution seismic information to accurately model the fluid movement in the reservoir, improve the forecast predictions and optimize the field development planning.

High-performance computing and runtime optimisation

The computational cost of running fine grid models used to be prohibitive. With the advances in computing technologies multimillion grid cell model runs are now possible. The

14.7 million simulation model was initially run with a standard server. The simulation run time on this standard equipment to simulate a 25-year forecast was ca. 11.5 hours. However, using CGG's high-performance computing (HPC) facilities at one of CGG's HPC centres the same model was run using a customized server which reduced the simulation runtime by a factor of 3.9. Faster simulation runtimes are possible using more HPC resources but using more resources would only translate to diminishing returns in terms of reduction of run-time.

Conclusions

CGG conducted high-resolution dynamic simulations of 14.7 million grid cells in the Måløy Slope area, using CGG's high-resolution seismic data, with the goal of improving understanding of the impact of small-/medium-scale heterogeneity on reservoir recovery as well as exploring utilization of this HFM for optimizing field development planning.

A base-case simulation model was configured with the same resolution as the seismic resolution in the areal direction (12m x 18.75 m) and with the vertical resolution of the well log data (1.25 m). The HFM produces more accurate results compared to coarser models for well recoverable volumes, plateau duration and water breakthrough time. The increased integration of seismic data adds realism to the dynamic modelling, helping to better define the well locations, estimate recoverable resources and well geometry (vertical vs horizontal wells), and optimise the development plan and production forecast. Other HFM model scenarios (low and high) can be history-matched to further assess uncertainty impact on plateau duration, WBT and recoverable resources.

The computational expense of a model increases with the number of grid cells, which in the past had made millions of grid cell models, a prohibited option for engineers. With large

advances in high-performance computing, model resolution can be increased to the level required to capture reservoir heterogeneities enabling full utilization of the information provided by the high-resolution seismic data. High-resolution dynamic models are therefore best used to explore where to drill new wells and to optimise development plans, focusing on incorporating detailed information on bypassed hydrocarbons. CGG's HPC state-of-the-art facilities allowed CGG to run these large models in a reasonable timeframe for decision-making.

References

- Coll, Carolina "Application of Probabilistic and Deterministic Methods for Consistent Reserves and Resources Estimation and Reporting." Paper presented at the SPE Europec featured at 81st EAGE Conference and Exhibition, London, England, UK, June 2019.
- Norwegian Petroleum Directorate [2022]. Delineation of oil and gas discovery near the Gjøa field in the North Sea – 35/9-16 S and 35/9-16 A — The Norwegian Petroleum Directorate (npd.no) (Link accessed 1st July 2022).
- Prélat, A. et al. [2015]. Constraining sub-seismic deep-water stratal elements with electrofacies analysis; A case study from the Upper Cretaceous of the Måløy Slope, offshore Norway. *Mar Petrol Geol*, 59, 268-285 (2015).
- Surlyk, F., Dons, T., Clausen, C.K. and Higham, J. [2003]. Upper Cretaceous. In: Evans, D., Graham, C., Armour, A. and Bathurst, P. (Eds.), *The Millennium Atlas: Petroleum Geology of the Central and Northern North Sea*. The Geological Society of London, London, pp. 213-233.
- Soubaras, R., Downle, R. and Sablon, R. [2012]. BroadSeis: Enhancing interpretation and inversion with broadband marine seismic. *CSEG Recorder*, Special Section: Seismic Acquisition, pp. 40-46.
- Norwegian Petroleum Directorate [2022]. Fact Page for well 35/3-2, Factor Page for well 35/3-4, Fact Page for well 35/3-7S (Link accessed 22nd July 2022).

ADVERTISEMENT





YOUNG PROFESSIONALS SUMMIT

17 NOVEMBER 2022 | ABERDEEN, LONDON & ONLINE

SAVE THE DATE!

